Chemical Vapor Deposition

DOI: 10.1002/cvde.201207030

Full Paper

# A Micro-pulse Process of Atomic Layer Deposition of Iron Oxide Using Ferrocene and Ozone Precursors and Ti-Doping

By *Xianglin Li*, *Ng Chin Fan*, and *Hong Jin Fan**

Hematite ($\alpha$-$Fe_2O_3$) thin films are obtained by atomic layer deposition (ALD) in the temperature range $200-350^{\circ}C$ using ferrocene and ozone as the precursors. A micro-pulse process facilitates the precursor adsorption and shortens the ferrocene dose time to 5 s. When tested on Si(100) substrates, the growth rate is around 0.5 Å per cycle for the first 300 cycles, after which the growth becomes nonlinear. Interestingly, a linear growth can be maintained with a rate of ≈0.55 Å per cycle by $TiO_2$ co-deposition (cycle ratio of $TiO_2/Fe_2O_3 = 1{:}20$). Characterizations by X-ray photoemission spectroscopy (XPS), Raman spectroscopy (RS), and UV-vis absorption confirm the presence of the $\alpha$-$Fe_2O_3$ phase after post-deposition annealing. Uniform depositions on dense ZnO nanorod arrays and anodic aluminum oxide (AAO) templates are also demonstrated, inferring that the current process is capable of coating on high (>50) aspect ratio structures.

Keywords: ALD, Ferrocene, Iron oxide, Micro-pulse, Ozone, $TiO_2$ doping

## 1. Introduction

Hematite ($\alpha$-$Fe_2O_3$) is the most common form of iron oxide, and has emerged as a promising photoelectrode material due to its favorable optical band gap (≈2.2 eV), chemical stability in aqueous environments, ample abundance, and low cost.[1–6] Recently, hematite has attracted wide interest in energy applications such as batteries[7,8] and photoelectrochemical cells for solar-fuel generation.[2,6,9] It has been theoretically predicted that a semiconductor with this band gap can achieve a solar-to-hydrogen efficiency of 16.8%,[9] however the reported efficiencies for $\alpha$-$Fe_2O_3$ are notoriously lower than the predicted value.[4,5,10] The poor performance was primarily attributed to a combination of very short hole diffusion length (≈10 nm) compared to the light penetration depth of several hundred nanometers.[4,6,10] To overcome the drawback, one possibility is to have a non-conventional photoelectrode design, which is characterized by both high surface areas and short charge-collection distances. Such a design will require techniques for controllable coating on pre-structured nano-templates. For this purpose, ALD stands out as the most convenient method due to its abilities in respect of conformal coating on arbitrary-shaped surfaces, and atomic control in film thickness. ALD is based on cyclic self-limiting deposition reactions that prevent precursor reactions above the substrate surface. Owing to the self-limiting nature of ALD, high aspect ratio structures, such as nanoparticles, nanowires, nanotubes, soft materials, and biological materials can be coated with thin films of oxides and nitrides or metal nanoparticles, that are not achievable by conventional physical or chemical vapor depositions.[11–13] The obtained low-dimensional nanostructures have been demonstrated in a wide range of applications, including catalysis, microelectronics, energy storage, and conversion and sensing.[12–17]

The first report on ALD-produced $\alpha$-$Fe_2O_3$ film was done by using *tris*-(2,2,6,6-tetramethyl-3,5-heptanedionate)iron(III) ($Fe(thd)_3$) and ozone ($O_3$) as precursors,[18] however the low growth rate (0.1 Å per cycle), and the small iron vapor pressure, limit its applicability to high aspect ratio structures. Subsequent reports of $Fe_2O_3$ deposition via ALD using ferrocene ($Fe(Cp)_2$) and oxygen as precursors required high temperatures ($\approx 350-500^{\circ}C$).[19,20] Also, ALD-produced $Fe_2O_3$ using *tert*-butoxide ($Fe_2(O^tBu)_6$) and water occurs only in a narrow temperature window ($\approx 130-170^{\circ}C$) and incites carbon incorporation.[21] Recently, Martinson et al.[22] reported on ALD-produced $Fe_2O_3$ using $Fe(Cp)_2$ and $O_3$ with a modulated lower temperature window ($\approx 200-350^{\circ}C$) which was capable of coating Si microtrenches with an aspect ratio of ≈150 using a longer dose time. The self-limiting growth kinetics and surface reaction mechanism were described therein. On the other hand, it was reported that the ALD of $Fe_2O_3$ using $Fe(Cp)_2$ and $O_3$ may show a decrease in growth rate after the first few hundred cycles,[23] thus elongating the overall deposition time. For the practical application of the ALD of $Fe_2O_3$, it is desirable to have a shortened dose time and linear growth mode (i.e., film thickness is proportional to the cycle number).

In this study, we describe a micro-pulse ALD process for growing $Fe_2O_3$ using $Fe(Cp)_2$ and $O_3$ precursors, and we explore the possibility of Ti-doping. As compared to the previous report, the micro-pulse process exhibits a

[*] X. L. Li, N. C. Fan, Prof. H. J. Fan
Division of Physics and Applied Physics, School of Physical and Mathematical Sciences, Nanyang Technological University, 21 Nanyang Link, 637371 (Singapore)
E-mail: fanhj@ntu.edu.sg

  

combination of lower precursor exposure and purge times, effectively faster growth speed, and the ability to coat high aspect ratio nanotemplates (nanorods and nanochannels). By introducing $TiO_2$ co-deposition, the commonly observed nonlinear growth rate of $Fe_2O_3$ can be prevented, and simultaneously, a controllable Ti-doping into $Fe_2O_3$ films can be achieved by adjusting the ALD cycle ratios of $TiO_2$ and $Fe_2O_3$. For their potential application in photoelectrochemical cells and lithium-ion batteries, uniform coating on non-planar substrates has also been attempted with success.

## 2. Results and Discussion

Due to the self-limiting nature of each half cycle, ALD is capable of conformal and uniform coating on both planar surfaces and high aspect ratio structures, with an atomic control of thickness. A true ALD process (i.e., without CVD side-reaction) will exhibit saturated surface reactions such that, with increasing precursor exposure, a plateau in the growth rate is observed. In our experiment, the exposure is strictly proportional to the dose time. For the micro-pulse process in this study, the dose time is equal to the pulse time multiplied by the pulse numbers (see Experimental section for details). Figure 1a shows the $Fe_2O_3$ growth rate at 250°C versus the precursor dose time. The growth rate was calculated from the $Fe_2O_3$ thin film on a Si(100) substrate over 200 ALD cycles. The film thickness was determined by spectroscopic ellipsometry (SE). It can be clearly seen that, after a dose time of 5 s, the growth rate curve starts to plateau, in good accordance with the self-limiting characteristics of an ALD reaction. The curve can be fitted to a Langmuir adsorption model, $Q = Q_m Kt/(1 + Kt)$, where $Q$ is the growth rate, $Q_m$ is the maximum growth rate, $K$ is the Langmuir coefficient, and $t$ is the dose time. The fitting results in $Q_m = 0.5$, $K = 1.5$. The saturate growth rate, 0.5 Å per cycle, is comparable to the previous report by Klahr et al. (0.6 Å per cycle),[23] but smaller than that (1.4 Å per cycle) in the recent report by Martinson et al.,[22] however in their work, the threshold dose time for $Fe(Cp)_2$ was 40 s and for ozone was 200 s, both much longer than the dose time we used (typically 10 s). Therefore, considering the shorter exposure and purge times, the overall growth speed in our experiment, which is 80 s for one full cycle (including 20 s $N_2$ purge) is effectively greater. For application in photoelectrochemical cells, in which the typical film thickness is around 10 nm, the deposition rate in our study is fairly acceptable.

There may be two reasons for the reduction of the threshold dose time for the micro-pulse process: First, a constant high $Fe(Cp)_2$ precursor pressure can be maintained during the micro-pulse process. In a micro-pulse process the $Fe(Cp)_2$ pressure can be maintained at about 13 mbar (Experimental Section), while for a normal, single-pulse process, the pressure drops quickly. Second, the precursors

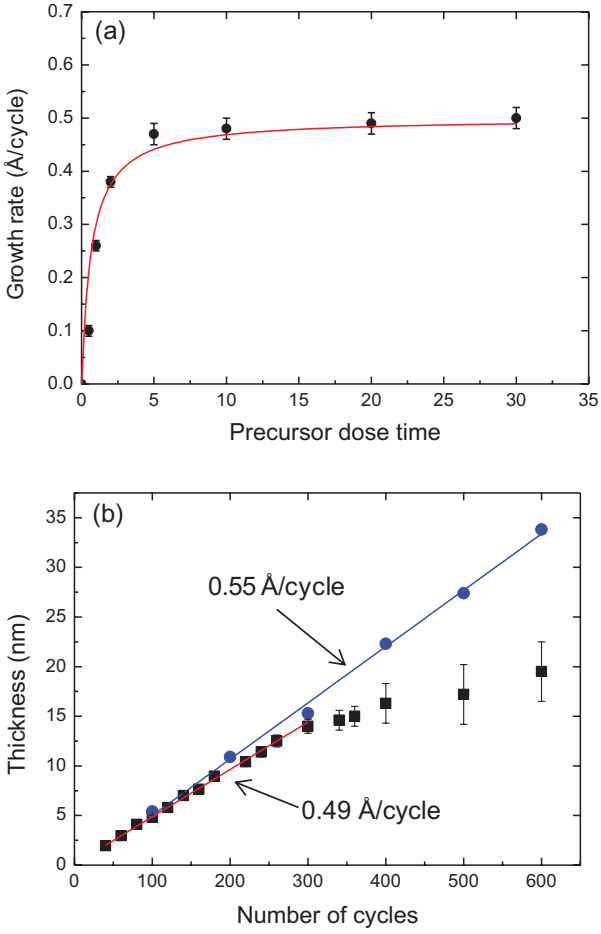


Fig. 1. a) $Fe_2O_3$ growth rate at 250°C versus the precursor dose time after 200 cycles. The growth rate is determined from the average film thickness on Si substrate located at the center of the reaction chamber during a single run. The solid line is the fit to the Langmuir adsorption model. b) $Fe_2O_3$ film thickness on Si substrate versus the number of $Fe(Cp)_2/O_3$ cycles using the dose time of 10-20-10-20 s (black curve). Shown also is the same plot for $TiO_2$ co-deposition with a cycle ratio of $TiO_2/Fe_2O_3 = 1{:}20$ at 250°C (blue curve). The solid lines are the best linear fits to the data.

enter the reaction chamber with a periodic disturbance, so that the gas flow passes the sample surface like a wave. As a result, the adsorption of precursor molecules on the sample surface could be improved.

A true ALD deposition is also characterized by a linear growth mode, i.e., film thickness is proportional to the cycle number. In our experiment, linear growth is observed on the Si(100) substrate for the first 300 cycles with both $Fe(Cp)_2$ and $O_3$ dose times of 10 s (Fig. 1b), and the growth rate is calculated to be 0.5 Å per cycle. After 300 cycles, the growth rate decreases and film thickness increases only slightly with further ALD cycles. This phenomenon has also been observed in the previous report.[23] One possible reason for the growth rate reduction is the decomposition of the $Fe(Cp)_2$ precursor. It has been reported that the decomposition of $Fe(Cp)_2$ can be accelerated due to Fe- and C-coated vessels.[24] Therefore, a self-catalytic process can

  

occur such that the decomposition product (containing Fe and C) might, in turn, accelerate the decomposition of $Fe(Cp)_2$ itself. Thus, the decomposition rate increases with ALD cycle number, resulting in a nonlinear growth. Interestingly, we found here that, by introducing one cycle of $TiO_2$ using $TiCl_4$ and $H_2O$ after each 20 $Fe_2O_3$ cycles, a linear growth can be obtained up to 600 cycles, resulting in a film thickness of 33 nm (see Fig. 1b). This linear growth could be related to an elimination of the self-decomposition of $Fe(Cp)_2$. The one-cycle $TiO_2$ layer might passivate the chamber and substrate surface and therefore retard the autocatalytic decomposition process. Therefore, the $TiO_2$ co-deposition can effectively maintain a constant growth rate, even at high cycle numbers. In the meantime, it also provides the opportunity for controllable Ti-doping by adjusting the cycle ratio of $TiO_2$ and $Fe_2O_3$.

It has been reported that the ALD of $Fe_2O_3$ using $Fe(Cp)_2$ and $O_3$ shows a distance-dependence of the growth rate.[22] This phenomenon was also checked and confirmed in our experiment, as shown in Figure 2. Along the precursor flow direction, the growth rate exhibits a slight decrease, a plateau, and a further decrease at positions measured away from the inlet point. The uniform range is about 16 cm, ≈75% of the chamber diameter. Along the direction perpendicular to the precursor flow, the uniform range is about 12 cm, ≈60% of the chamber size. Several mechanisms have been proposed to account for such distance-dependence.[22] One of them is related to the decomposition of precursors in the reactor chamber. The decomposition may produce a precursor concentration gradient, so that the precursor concentration in the gaseous phase drops both along the flow direction and in the perpendicular direction away from the center. The lower gradient regions will have a lower growth rate. In addition, a catalytic decomposition of ozone over the $Fe_2O_3$ surface is also possible, which will also generate an $O_3$ concentration gradient away from the chamber center.[25]

In order to evaluate the ALD temperature window, $Fe_2O_3$ films were deposited in the temperature range 160 – 325°C. The precursor dose time was fixed at 10 s. Figure 3 shows the dependence of growth rate on deposition temperature. It clearly shows that, for temperatures higher than 200°C, the growth rate shows a plateau, while when the temperature is lowered to 160°C, there is barely any ALD growth. Deposition at temperatures higher than 325°C was not attempted, as it reaches the ALD temperature of $Fe(Cp)_2$ and oxygen for $Fe_2O_3$.[19] Therefore, in our study, the ALD window can be expected at ≈200 – 325°C, similar to the previous report.[22] A photograph of one representative sample of the as-deposited $Fe_2O_3$ film on a glass substrate (Fig. 3 inset) shows a red-orange color.

XPS was used to verify the $Fe_2O_3$ phase and Ti incorporation. Figure 4a shows the survey scan from both pure and $TiO_2$ co-deposited ALD-produced $Fe_2O_3$ films. Both spectra show the same features of $Fe_2O_3$ in Fe 2p and the existence of O, but only the $TiO_2$ co-deposited sample shows the Ti element. Figures 4b and c show the details of the Fe 2p and Ti 2p peaks, respectively. The peaks of the Fe $2p_{1/2}$ and Fe $2p_{3/2}$ for the pure $Fe_2O_3$ and $TiO_2$-doped films are almost the same. The binding energies of Ti $2p_{1/2}$ and Ti $2p_{3/2}$ are observed at 464.3 and 458.5 eV, respectively, indicating a normal state of $Ti^{4+}$ in the anatase $TiO_2$. These binding energies are fully consistent with values reported for $TiO_2$.[26–28] Therefore, it could be inferred that the one cycle $TiO_2$ co-deposition has little effect on the chemical state of Fe. The increase in the $Fe_2O_3$ growth rate (Fig. 1b) could be due to the addition of $TiO_2$ itself, which was excluded in the calculations of growth rate.

Raman spectroscopy is widely used to analyze the phase of iron oxides due to the distinct spectra of various crystal

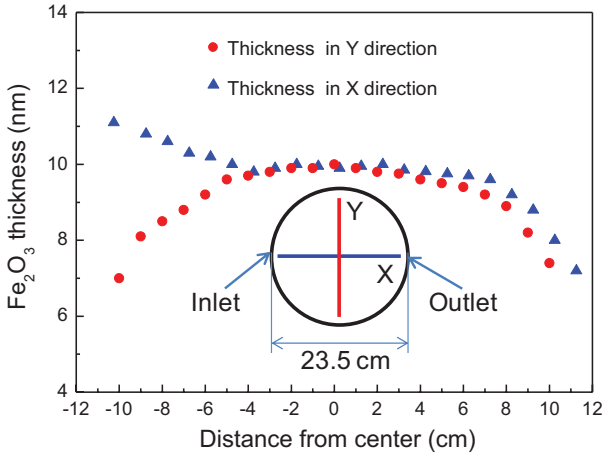


Fig. 2. Distance-dependence of the ALD growth rate inside the reaction chamber. Triangle curve (blue): $Fe_2O_3$ film thickness measured at various locations away from the precursor inlet and along the precursor flow direction. Circle curve (red): $Fe_2O_3$ film thickness at various locations away from the center and perpendicular to the precursor flow direction. The precursor dose time is 10-20-10-20 s and cycle number is 200. The deposition temperature is 250°C.

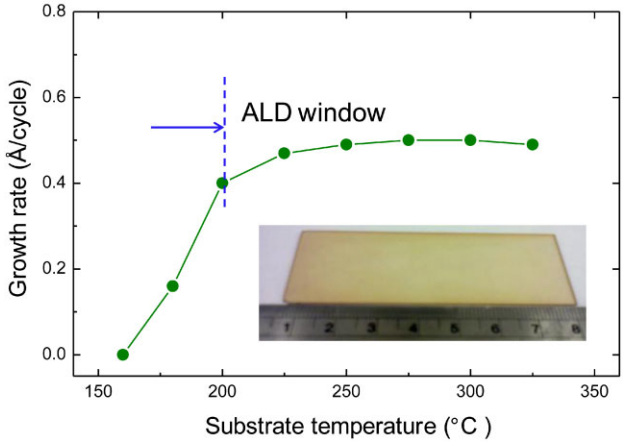


Fig. 3. $Fe_2O_3$ growth rate on Si(100) substrate versus the deposition temperature (200 cycles) using dose time 10-20-10-20 s. The potential ALD window for $Fe_2O_3$ growth is indicated. Inset: A photograph of $Fe_2O_3$ film deposited on a glass slide at 250°C.

  

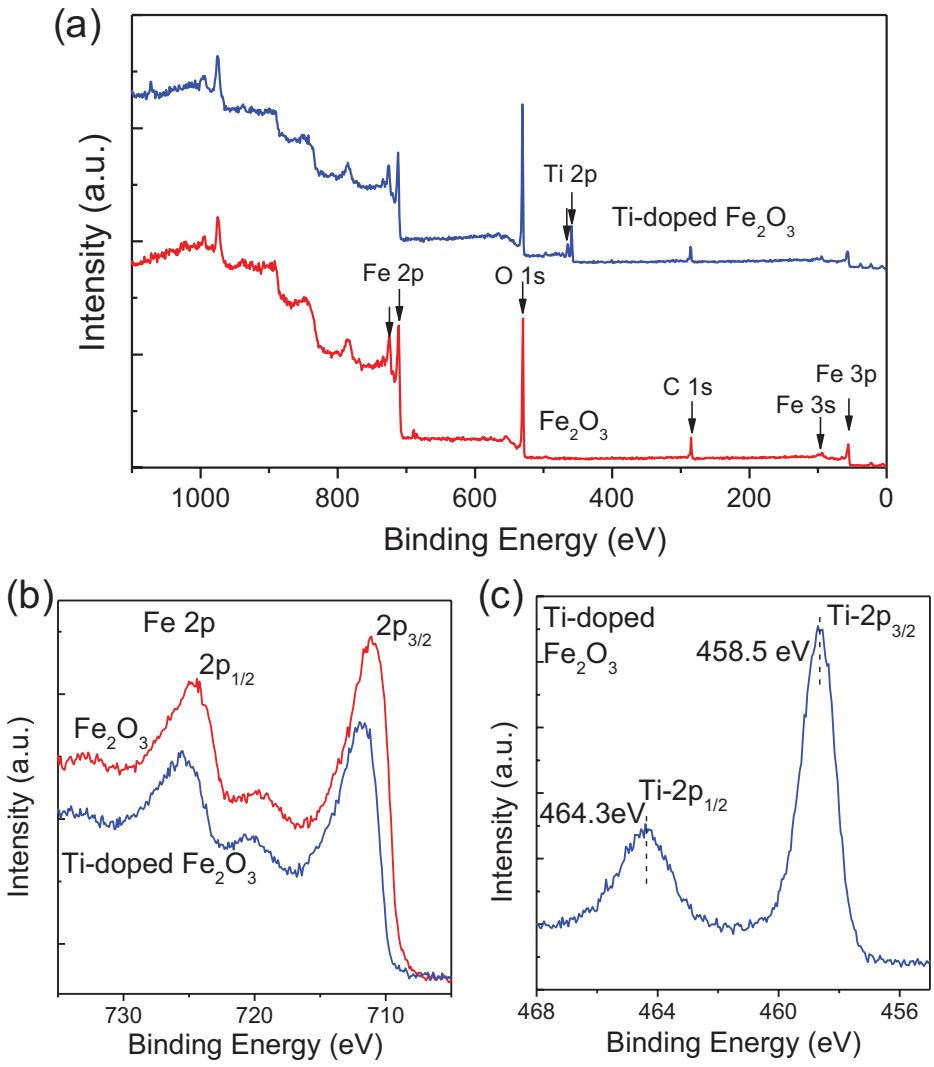


Fig. 4. a) XPS survey scan of pure, and $TiO_2$ co-deposited, ALD-produced $Fe_2O_3$ thin films on Si substrates. b) Fe 2p details for both samples. c) Ti 2p chemical states for the $TiO_2$ co-deposited film.

phases, hematite ($\alpha$-$Fe_2O_3$), maghemite ($\gamma$-$Fe_2O_3$), and magnetite ($Fe_3O_4$). Figure 5a shows the Raman spectra of the 20 nm ALD-produced $Fe_2O_3$ film deposited on a fluorine-doped tin oxide (FTO) substrate before and after thermal annealing. The as-deposited film shows no distinguishable Raman peaks because of its amorphous (or poor crystalline) structure. After post-annealing at 500°C for 1 h, the typical Raman peaks of $\alpha$-$Fe_2O_3$ at 225, 293, 403, and 1318 $cm^{-1}$ are observed, consistent with the previous report.[29] The two peaks at 600 and 1100 $cm^{-1}$ come from the FTO substrate. No peak from other iron oxide phases can be detected, implying that the crystal phase of the ALD-produced iron oxide using ferrocene and ozone, after post annealing, is dominantly hematite. Note that, due to the small thickness, X-ray diffraction (XRD) characterization was not attempted as it is not expected to show features related to hematite. Figure 5b shows the UV-vis absorption spectra of the 20 nm thick ALD-produced hematite thin films grown on the FTO substrate. The absorption onset at around 600 nm of the pure $Fe_2O_3$ sample is consistent with a $\approx$2.1 – 2.2 eV band gap of hematite reported in many other studies,[30–33] while for the sample with $TiO_2$ co-deposition, the absorption edge blue shifts slightly, accompanied by a decrease in the absorptance.

The above results confirm that the obtained $Fe_2O_3$ films are pure $Fe_2O_3$, and there is a high possibility of Ti-doping by the $TiO_2$ co-deposition, similar to the widely studied Al-doping in ZnO by ALD. Co-deposition with other $Fe_2O_3$/$TiO_2$ ratios of 5:1, 10:1, and 40:1 were also conducted in which the $Fe_2O_3$ ALD cycles were fixed at 300. The obtained film thicknesses are 32.4, 22.1, and 15.4 nm, respectively. It has been reported that the photocurrent onset potential of Ti-doped $Fe_2O_3$ can be shifted about 0.1 – 0.2 V to a lower value compared to an undoped sample.[28] The doping will improve the photocurrent and the photon-to-current conversion efficiency at lower bias voltages.[28] It will be

  

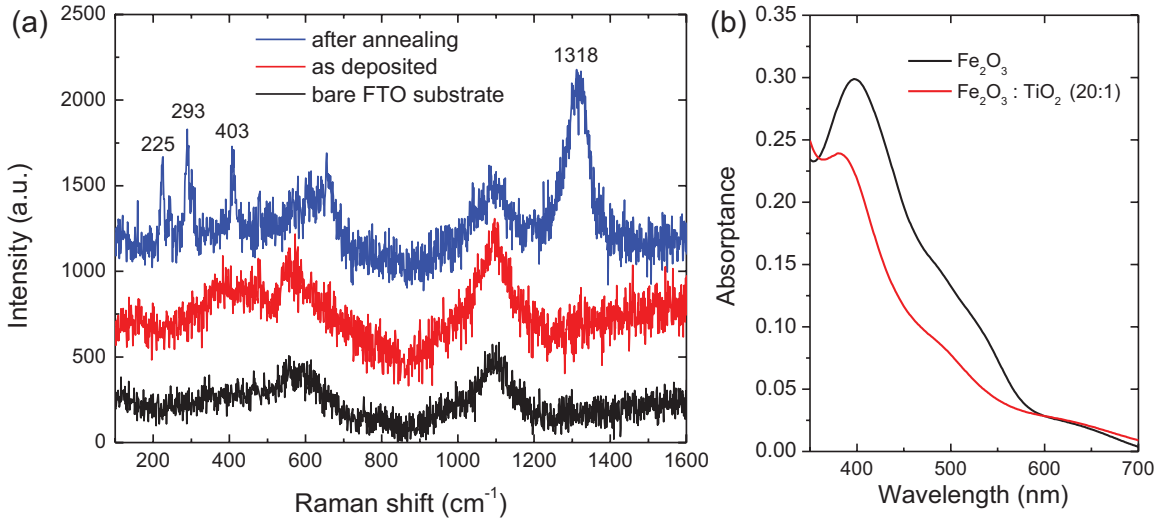


Fig. 5. a) Raman spectra of the as-deposited 20 nm thick $Fe_2O_3$ film on FTO substrate (red curve) and after 500°C annealing (blue curve). b) UV-vis absorption spectra of the 20 nm thick $Fe_2O_3$ film deposited on FTO substrate with, and without, $TiO_2$ co-deposition.

of interest to explore the controlled Ti-doping of $Fe_2O_3$ by ALD for application in solar energy conversion devices.

Conformal coating of high aspect ratio structures is essential to the application of $Fe_2O_3$ in photoelectrochemical devices, for which a continuous electrical path needs to be established along the long dimension. For demonstration, both positive and negative templates were tested using the micro-pulse process. Figure 6 shows the scanning electron microscopy (SEM) images of the ZnO nanorods array and anodic aluminum oxide (AAO) template after ALD-produced $Fe_2O_3$. Details of the hydrothermal growth of the ZnO nanorods can be found elsewhere.[34] The aspect ratio of the ZnO nanorods is about 20 (Fig. 6a). After 500 cycle ALD (with $TiO_2$ co-deposition), the conformal coating of the nanorods can be clearly seen (Fig. 6b); the average diameter of the ZnO nanorods increases from 80 to 130 nm,

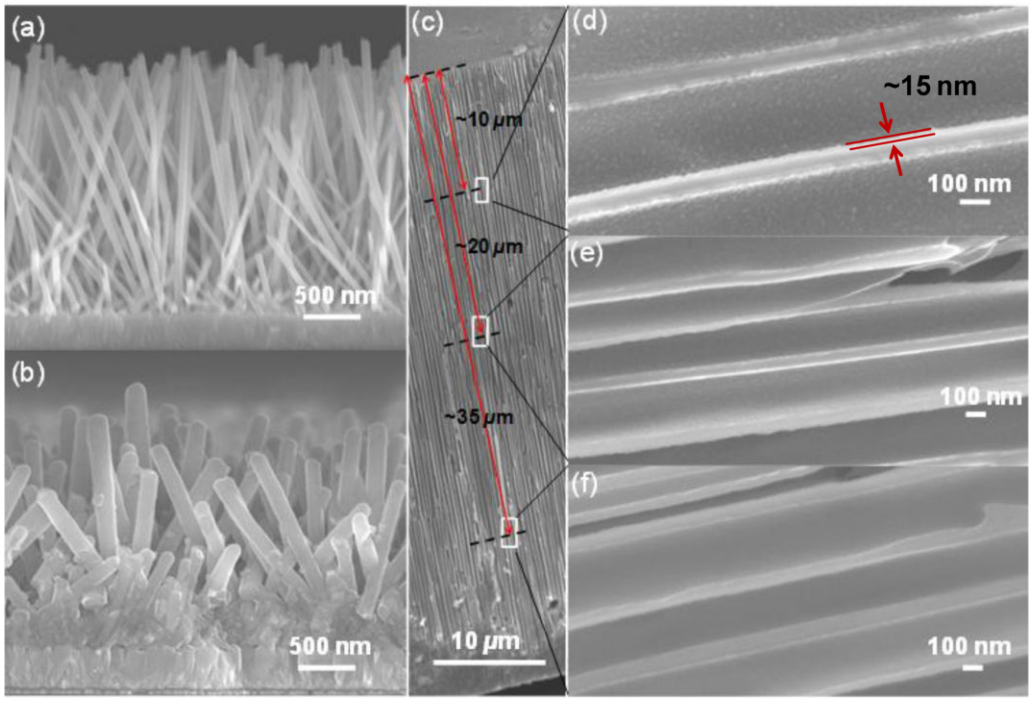


Fig. 6. ALD-produced $Fe_2O_3$ on non-planar substrates. SEM images of a) pristine ZnO nanorods array and b) after ≈25 nm thick $Fe_2O_3$ deposition at 250°C with the dose time of 10-20-10-20 s. c) SEM image of a 45 μm thick AAO template (pore size 300 nm) after $Fe_2O_3$ deposition at 250°C with dose time of 30-30-30-30 s. d-f) Enlarged views at various parts of the cross-section of c).

  

Chemical Vapor Deposition

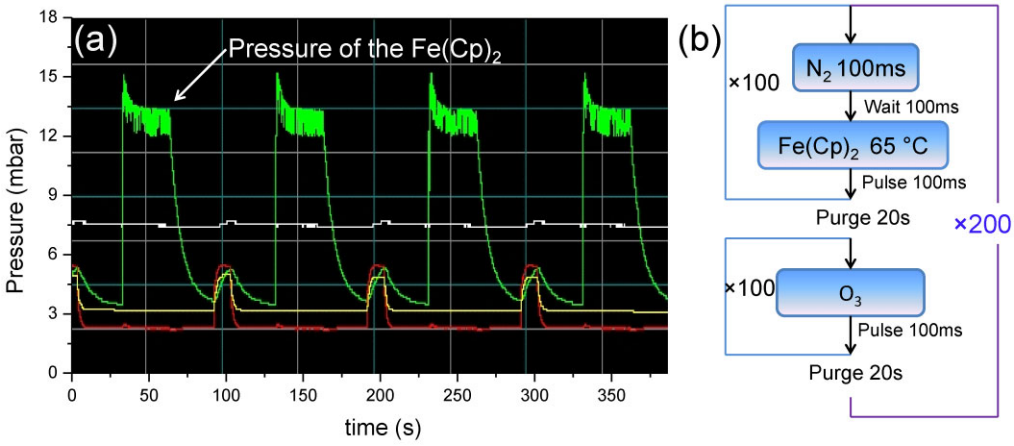


Fig. 7. a) *In-situ* $Fe(Cp)_2$ pressure during the micro-pulse process. b) Flow chart of the precursor delivery for the micro-pulse process for $Fe_2O_3$ deposition.

corresponding to a thickness of the $Fe_2O_3$ layer of about 25 nm. The clogging at the bottom is a result of smaller gaps between the ZnO nanorods near the substrate surface, which is a common phenomenon in the hydrothermal growth of ZnO nanorods. For the AAO template with 300 nm diameter pores and a total depth of 45 μm, a longer dose time was used. Figure 6c shows the cross-section of a 300 cycle ALD $Fe_2O_3$-coated AAO template with a dose time of 30-30-30-30 s. Figures 6d-f show the cross-section of the portion with the approximate distance of 10, 20, and 35 μm from the top, respectively. A uniform layer of $Fe_2O_3$ with a thickness of about 15 nm can be seen down to 10 μm. At a depth of 20 μm, however, only discrete small particles can be observed, and near the bottom no $Fe_2O_3$ deposition is achieved. Therefore, with a 30 s dose time, a uniform coating of porous structures with an aspect ratio of about 50 can be achieved with such a micro-pulse process.

## 3. Conclusions

Hematite ($\alpha$-$Fe_2O_3$) has been deposited by ALD based on a micro-pulse process using ferrocene and ozone precursors. Typical ALD behavior is observed over a temperature range between 200 and 325°C. The micro-pulse process exhibits a shorter precursor dose time (about 10 s for both precursors), a growth rate of ≈0.5 Å per cycle, and the capability of conformal coating on structures with aspect ratios >50. By introducing $TiO_2$ co-deposition to $Fe_2O_3$ with a cycle ratio of 1:20, the previously observed decrease in the growth rate after the first hundred cycles can be prevented, and simultaneously, Ti-doping is achievable. The hematite film deposited on a FTO substrate exhibits an optical band gap of about 2.1 eV. Uniform coating on high aspect ratio structures, including dense arrays of ZnO nanorods and AAO template, have also been demonstrated. The obtained hematite films on 3D substrates may find applications in lithium-ion batteries and photoelectrochemical devices.

## 4. Experimental

*ALD of $Fe_2O_3$ and $TiO_2$*: ALD of $Fe_2O_3$ was conducted based on a Beneq TFS-200 system using $Fe(Cp)_2$ (Aldrich, >98%) and $O_3$ (≈300 sccm ultrahigh purity $O_2$, BMT 830N) as the iron and oxygen sources, respectively. The $Fe(Cp)_2$ was held in a stainless steel bottle maintained at 65°C, while the reaction chamber was heated to 250°C. High purity $N_2$ gas was the process gas. During the deposition, the reaction chamber was maintained at 2 mbar with a steady $N_2$ stream at 250 sccm. In the micro-pulse process, the dose time is equal to the pulse time multiplied by the pulse numbers. Typically, each $Fe(Cp)_2$ half cycle consists of 100 × (100 ms filling of $N_2$ + 100 ms wait time + 100 ms pulse time). During the filling and waiting times the precursor valve was closed. In this definition, the dose time for $Fe(Cp)_2$ is 100 ×100 ms = 10 s. During this exposure process the pressure of $Fe(Cp)_2$ is maintained at about 13 mbar, as shown in Figure 7a. Each $O_3$ precursor exposure consists of 100 × 100 ms pulse time. Between the $Fe(Cp)_2$ and $O_3$ exposure, a 20 s purge with $N_2$ was used. Figure 7b shows the flow chart of precursor sequences of the micro-pulse process. For convenience, the ALD timing sequences was expressed as $t_1$-$t_2$-$t_3$-$t_4$, where $t_1$ is the dose time for $Fe(Cp)_2$, $t_2$ is the purge time following the first exposure, $t_3$ is the dose time for $O_3$, and $t_4$ is the purge time following the $O_3$ exposure. ALD of $TiO_2$ was conducted at 250°C using $TiCl_4$ and $H_2O$ as the precursors, and the precursor dose time was 200 ms for both $TiCl_4$ and $H_2O$ with 1 s $N_2$ purge in between.

*Characterization*: The morphology of the as-fabricated samples was characterized using a JEOL JSM-6700F field emission SEM. The $Fe_2O_3$ film thickness on the Si substrate was measured using a SE ($\alpha$-SE, J. A. Woollam). The Cauchy fitting model and refractive indices used for fitting were provided by J. A. Woollam. The UV-vis absorption spectra of $Fe_2O_3$ films on glass slides were recorded using a microspectrophotometer (Craic 2000). Raman measurements were conducted with a Renishaw system using a 532 nm laser as the excitation source. The as-deposited thin films were annealed in a quartz-tube furnace with both ends open at 500°C for 1 h.

Received: November 1, 2012
Revised: December 12, 2012

[1] A. Duret, M. Grätzel, *J. Phys. Chem. B* **2005**, *109*, 17184.
[2] K. Sivula, F. LeFormal, M. Grätzel, *ChemSusChem* **2011**, *4*, 432.
[3] Y. Lin, G. Yuan, S. Sheehan, S. Zhou, D. Wang, *Energy Environ. Sci.* **2011**, *4*, 4862.
[4] T. Lindgren, H. L. Wang, N. Beermann, L. Vayssieres, A. Hagfeldt, S. E. Lindquist, *Sol. Energy Mater. Sol. Cells* **2002**, *71*, 231.
[5] U. Bjorksten, J. Moser, M. Gratzel, *Chem. Mater.* **1994**, *6*, 858.
[6] N. Beermann, L. Vayssieres, S. E. Lindquist, A. Hagfeldt, *J. Electrochem. Soc.* **2000**, *147*, 2456.
[7] J. Jiang, Y. Li, J. Liu, X. Huang, C. Yuan, X. W. Lou, *Adv. Mater.* **2012**, *24*, 5166.

  

[8] Y.-M. Lin, P. R. Abel, A. Heller, C. B. Mullins, *J. Phys. Chem. Lett.* **2011**, *2*, 2885.

[9] A. B. Murphy, P. R. F. Barnes, L. K. Randeniya, I. C. Plumb, I. E. Grey, M. D. Horne, J. A. Glasscock, *Int. J. Hydrogen Energy* **2006**, *31*, 1999.

[10] J. H. Kennedy, K. W. Frese, *J. Electrochem. Soc.* **1978**, *125*, 1999.

[11] M. Knez, K. Nielsch, L. Niinistö, *Adv. Mater.* **2007**, *19*, 3425.

[12] C. Marichy, M. Bechelany, N. Pinna, *Adv. Mater.* **2012**, *24*, 1017.

[13] M. N. Liu, X. L. Li, S. K. Karuturi, A. I. Y. Tok, H. J. Fan, *Nanoscale* **2012**, *4*, 1522.

[14] X. L. Li, Y. Z. Zhang, Z. X. Shen, H. J. Fan, *Small* **2012**, *8*, 2548.

[15] C. Cheng, S. K. Karuturi, L. Liu, J. Liu, H. Li, L. T. Su, A. I. Y. Tok, H. J. Fan, *Small* **2012**, *8*, 37.

[16] Y. Lin, Y. Xu, M. T. Mayer, Z. I. Simpson, G. McMahon, S. Zhou, D. Wang, *J. Am. Chem. Soc.* **2012**, *134*, 5508.

[17] Y. Lin, S. Zhou, S. W. Sheehan, D. Wang, *J. Am. Chem. Soc.* **2011**, *133*, 2398.

[18] M. Lie, H. Fjellvåg, A. Kjekshus, *Thin Solid Films* **2005**, *488*, 74.

[19] M. Rooth, A. Johansson, K. Kukli, J. Aarik, M. Boman, A. Hårsta, *Chem. Vap. Deposition* **2008**, *14*, 67.

[20] J. R. Scheffe, A. Francés, D. M. King, X. Liang, B. A. Branch, A. S. Cavanagh, S. M. George, A. W. Weimer, *Thin Solid Films* **2009**, *517*, 1874.

[21] J. Bachmann, J. Jing, M. Knez, S. Barth, H. Shen, S. Mathur, U. Gösele, K. Nielsch, *J. Am. Chem. Soc.* **2007**, *129*, 9554.

[22] A. B. F. Martinson, M. J. DeVries, J. A. Libera, S. T. Christensen, J. T. Hupp, M. J. Pellin, J. W. Elam, *J. Phys. Chem. C* **2011**, *115*, 4333.

[23] B. M. Klahr, A. B. F. Martinson, T. W. Hamann, *Langmuir* **2010**, *27*, 461.

[24] L. M. Dyagileva, V. P. Mar'in, E. I. Tsyganova, G. A. Razuvaev, *J. Organomet. Chem.* **1979**, *175*, 63.

[25] B. Dhandapani, S. T. Oyama, *Applied Catalysis B: Environmental* **1997**, *11*, 129.

[26] D. Briggs, M. P. Seah, *Auger and X-Ray Photoelectron Spectroscopy: Practical Surface Analysis*, Wiley, New York 1990, Vol. 1, Appendix 1.

[27] J. F. Moulder, W. F. Stickle, P. E. Sobol, K. D. Bomben, in: *Handbook of X-ray Photoelectron Spectroscopy* (Ed: J. Chastain), Perkin-Elmer Corporation, Physical Electronics Division, Eden Prairie, MN 1992.

[28] G. Wang, Y. Ling, D. A. Wheeler, K. E. N. George, K. Horsley, C. Heske, J. Z. Zhang, Y. Li, *Nano Lett.* **2011**, *11*, 3503.

[29] D. L. A. de Faria, S. Venâncio Silva, M. T. de Oliveira, *J. Raman Spectrosc.* **1997**, *28*, 873.

[30] L. A. Marusak, R. Messier, W. B. White, *J. Phys. Chem. Solids* **1980**, *41*, 981.

[31] H. H. Kung, H. S. Jarrett, A. W. Sleight, A. Ferretti, *J. Appl. Phys.* **1977**, *48*, 2463.

[32] B. Gilbert, C. Frandsen, E. R. Maxey, D. M. Sherman, *Phys. Rev. B* **2009**, *79*, 035108.

[33] S. Mohanty, J. Ghose, *J. Phys. Chem. Solids* **1992**, *53*, 81.

[34] C. Cheng, B. Liu, H. Yang, W. Zhou, L. Sun, R. Chen, S. F. Yu, J. Zhang, H. Gong, H. Sun, H. J. Fan, *ACS Nano* **2009**, *3*, 3069.

  